ACS APPLIED MATERIALS & INTERFACES

Research Article

www.acsami.org

Activated Carbon Spheres for CO_2 Adsorption

Nilantha P. Wickramaratne and Mietek Jaroniec*

Department of Chemistry and Biochemistry, Kent State University, Kent, Ohio 44242, United States

Supporting Information

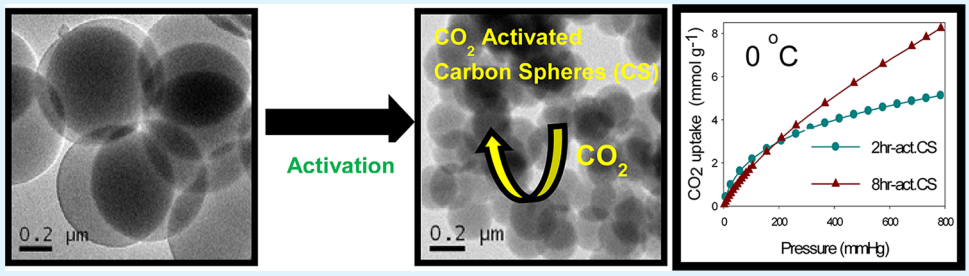

ABSTRACT: A series of carbon spheres (CS) was prepared by carbonization of phenolic resin spheres obtained by the one-pot modified Stöber method. Activated CS (ACS), having diameters from 200 to 420 nm, high surface area (from 730 to 2930 m^2/g), narrow micropores (<1 nm) and, importantly, high volume of these micropores (from 0.28 to 1.12 cm^3/g), were obtained by CO_2 activation of the aforementioned CS. The remarkably high CO_2 adsorption capacities, 4.55 and 8.05 mmol/g, were measured on these AC spheres at 1 bar and two temperatures, 25 and 0 °C, respectively.

KEYWORDS: *activated carbon spheres, CO_2 adsorption, CO_2 activation, Stöber method*

INTRODUCTION

The climate worsening observed in the recent years, caused probably by global warming, is the subject of a widespread public concern. The CO_2 emission associated with anthropogenic activities plays a big role in the global warming and climate change; therefore, extensive research efforts have been undertaken worldwide to develop feasible materials for CO_2 capture. It has been reported that the global atmospheric CO_2 concentration has increased from a preindustrial value of ~280 to 390 ppmv currently.[1] The main contributors to the observed CO_2 increase are vehicular emissions, fossil fuel-fired power plants, deforestation, and chemical processes. Among them, fossil fuel-fired power plants contribute 77% to the anthropogenic CO_2 emission totaling 38 Gt in 2004;[1−3] this value continues to grow every year. About a 50% increase in the CO_2 emission is expected from fossil fuel-fired power plants alone by 2030.

In the past decade, various types of adsorbents including zeolites,[4−6] metal organic frameworks (MOF),[7−10] functionalized porous silica,[11−13] porous polymers,[14,15] metal oxides,[16−18] and carbonaceous materials[19,20] have been examined for CO_2 capture. Among them, MOF and nanoporous carbons have gained much attention. It was shown that MOFs exhibit comparatively high CO_2 adsorption capacities up to 8.5 mmol/g[21] at ambient conditions (1 bar, 25 °C) and very high CO_2 uptake up to 54.5 mmol/g[22] at high pressures (50 bar) and 25 °C. Despite the excellent adsorption capacities of MOFs, these materials are much more expensive than the majority of carbonaceous adsorbents, especially commercially available activated carbons. In addition, MOFs are water sensitive;[23] they can chemisorb water, and/or their porous structure can be destroyed upon exposure to water vapor. Flue gas contains a considerable amount of water vapor; thus, MOFs are unlikely to be used in fossil fuel-fired power plants as CO_2 adsorbents unless they have significant improvement toward water stability. Due to the aforementioned reasons, MOFs are less feasible from the viewpoint of industrial applications. In contrast, carbonaceous adsorbents exhibit several advantages such as higher resistance to water due to their hydrophobicity, higher thermal stability, good chemical resistance to both alkaline and acidic media, easy preparation, tunable pore structure, low energy requirement for regeneration, and most importantly, low cost. Thus, carbonaceous materials are considered to be one of the most promising adsorbents for CO_2 capture.

Recently, numerous carbon materials, including activated carbons,[24] metal−carbon composites, biowaste derived carbons,[25,26] and nitrogen-doped carbons[27,28] have been thoroughly investigated for CO_2 adsorption. Most of these investigations have been done with a special emphasis on the development of high surface area microporous carbons and/or the incorporation of basic species, mainly nitrogen-containing groups into carbons. However, recent experimental and computer modeling studies[29,30] have shown that the carbons with fine micropores are needed to maximize the CO_2 adsorption capacity. Presser et al.[31] and Hu et al.[29] studied the CO_2 uptake on microporous carbons in relation to the pore size. They have also pointed out that the micropores smaller than 1 nm are responsible for high CO_2 adsorption at 1 bar. Also, our previous studies showed that the KOH activation of polymer spheres gave carbons with a high volume of fine micropores (<0.8 nm) able to adsorb the

Received: January 9, 2013
Accepted: February 11, 2013
Published: February 11, 2013

unprecedented CO_2 amounts up to 4.6 and 8.9 mmol/g at 23 and 0 °C under atmospheric pressure, respectively.[32]

This work shows that the carbon spheres obtained by a slightly modified Stöber recipe[33] and subjected to CO_2 activation featured a high fraction of fine micropores (<1 nm) and, consequently, high CO_2 adsorption capacity at ambient conditions. Namely, the CO_2 adsorption capacity of these activated carbon spheres reached, respectively, 4.55 and 8.05 mmol/g at 25 and 0 °C under atmospheric pressure (1 bar). The diameter of these spheres was in the range between 200 and 420 nm. This study provides further experimental evidence on the importance of fine micropores for high CO_2 uptake under ambient conditions.

EXPERIMENTAL SECTION

Synthesis of Carbon Spheres. Monodisperse carbon spheres (CS) were synthesized using a recipe reported by Liu et al.[33] The synthesis recipe used was as follows: an aqueous-alcoholic solution was prepared by mixing 48 mL of ethanol and 120 mL of distilled water at 30 °C. Subsequently, 0.6 mL of 25 wt % ammonia was added under continuous stirring. Then, 1.2 g of resorcinol was added and stirred until its complete dissolution. Next, 1.68 mL of 37 wt % formaldehyde was added slowly to the solution and stirred for 24 h at respective temperatures. Finally, the reaction mixture was transferred to three 125 mL capacity Teflon containers and placed in sealed metal autoclave vessels. Then, the vessels were placed in an oven at 100 °C for 24 h. The solid product (polymer spheres) was obtained by centrifugation and dried at 100 °C for 12 h.

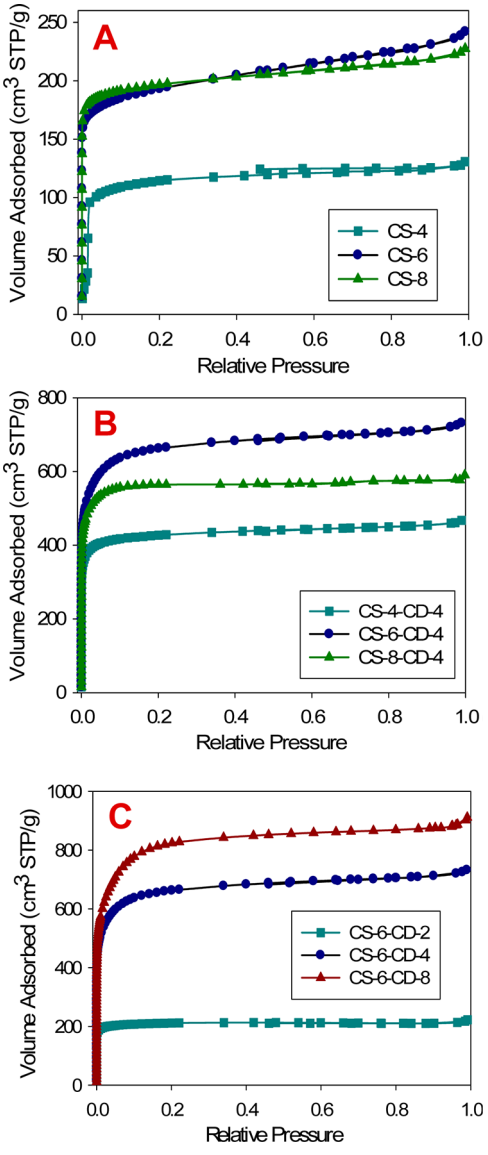

Figure 1. Nitrogen adsorption isotherms for CS-T series (A), CS-T-CD-4 series (B), and CS-T-CD-t series (C).

Table 1. Adsorption Parameters and Particle Size for Sample Studied[a]

sample	particle size (nm)	S_{BET} (m^2/g)	V_{total} (cm^3/g)	$PV_{1\ nm}$ (cm^3/g)	n_{CO2} (mmol/g) 25 °C	0 °C
CS-4		390	0.17		1.40	
CS-6	570	661	0.30	0.21	2.51	
CS-8		669	0.29	0.23	3.02	
CS-4-CD-4		1453	0.56	0.41	3.60	7.02
CS-6-CD-4	420	2284	0.89	0.43	4.55	7.48
CS-8-CD-4		1924	0.75	0.42	3.85	6.20
CS-6-CD-2		730	0.31	0.24	3.60	5.10
CS-6-CD-8	370	2930	1.12	0.43	4.40	8.05
CS-6-CD-12	200					

[a]Notation: V_{total} is the single point pore volume calculated from adsorption isotherm at P/P_o = 0.98; S_{BET} is the BET specific surface area obtained from the adsorption data in the P/P_o range from 0.05 to 0.2; $PV_{1\ nm}$ is the cumulative pore volume calculated in the range of pore widths up to 1 nm; n_{CO2} is CO_2 adsorption capacity at 25 and 0 °C and 1 bar.

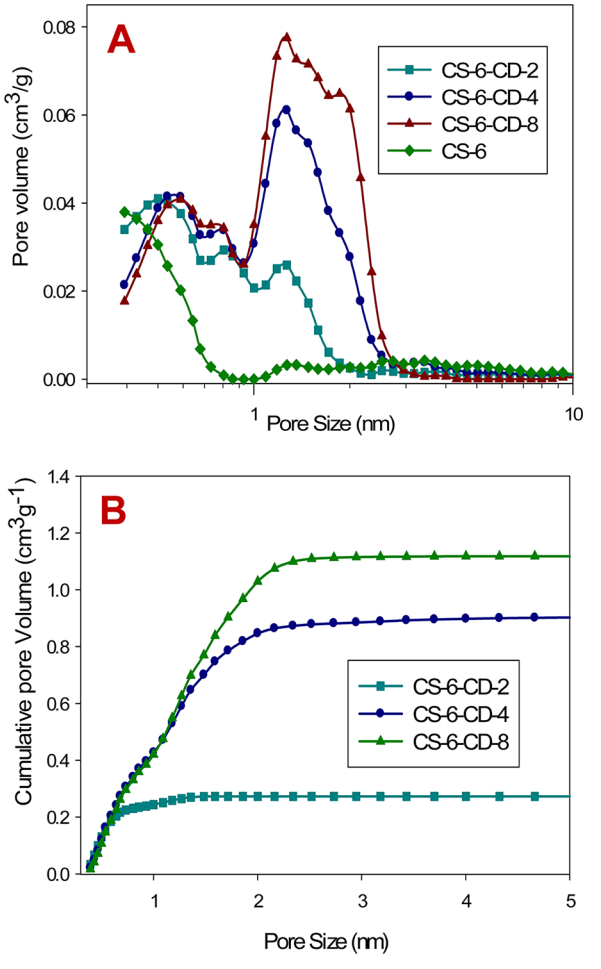

Figure 2. Pore size distribution curves (A) and cumulative pore volume plotted against pore width (B) for CS-6-CD-t series.

dx.doi.org/10.1021/am400112m | ACS Appl. Mater. Interfaces 2013, 5, 1849−1855

The carbon spheres obtained by carbonization of the aforementioned polymer spheres at 600 °C were prepared as follows: the latter were carbonized under flowing nitrogen in a tube furnace using heating rate of 1 °C/min up to 350 °C, dwell for 2 h, and resuming heating rate of 1 °C/min up to 600 °C and dwell for 4 h. The resulting carbon materials were labeled as CS-T, where "CS" refers to carbon spheres and "T" refers to the initial number of the three digit carbonization temperature; for instance, for the carbons obtained at 400, 600, and 800 °C T = 4, 6, and 8, respectively.

Activation of Carbon Spheres. The postsynthesis activation for carbon spheres was performed by placing a ceramic boat with 0.10 g of CS in a ceramic tube furnace under flowing nitrogen with a heating rate of 10 °C/min up to 850 °C. After reaching this temperature, the activating gas was introduced to the tube furnace (50 cm^3/min) for 2–12h and then switched back to nitrogen to prevent further activation during the cooling process. The obtained activated materials are denoted as CS-T-CD-t, where "T" represents the initial number of carbonization temperature expressed in °C, "CD" refers to activation gas (carbon dioxide), and "t" is the activation time in hours. Activation of all samples was performed at 850 °C.

Measurements and Characterization. TEM images were obtained using FEI Tecnai F20ST/STEM instrument operated at 200 keV. The preparation of samples for TEM analysis involved their sonication in ethanol for 2 to 5 min and deposition on a 400 mesh lacy carbon coated copper grid. Nitrogen adsorption isotherms were measured at −196 °C on ASAP 2010 volumetric adsorption analyzers manufactured by Micromeritics (Norcross, GA, USA) using nitrogen of 99.998% purity. CO_2 adsorption isotherms were obtained at both 0 and 25 °C on ASAP 2020 volumetric adsorption analyzer manufactured by Micromeritics. Before adsorption measurements, each sample was degassed under vacuum for at least 2 h at 200 °C. The specific surface area of the samples was calculated using the Brunauer–Emmett–Teller (BET) method within the relative pressure range of 0.05–0.20. Incremental pore size distributions were calculated from nitrogen adsorption data by the DFT method provided by Micromeritics. The thermogravimetric (TG) measurements were performed on a TA Instruments TGA Q500 thermogravimetric analyzer using a high-resolution mode. The X-ray diffraction (XRD) measurements were recorded for the carbonized samples using a PANanalytical, Inc. X'Pert Pro (MPD) Multi-Purpose Diffractometer with Cu Kα radiation (1.5406 Å) at an operating voltage of 45 kV.

RESULTS AND DISCUSSION

BET Surface Area and Pore Size Distributions (PSD). According to the recent studies,[32] microporous carbon with fine pores (<1 nm) are shown to have high CO_2 capture at ambient temperatures and pressures. It was also shown that the KOH activation of polymer spheres obtained by the Stöber method destroyed their spherical morphology but afforded microporous carbon materials with high fraction of fine pores (less than 1 nm). In the same report,[32] it was also shown that the activation of carbon spheres with aqueous KOH was not effective due to the lack of penetration of these hydrophobic spheres by KOH. In this study, we demonstrate that a simple CO_2 activation of phenolic resin-based carbon spheres at 850 °C for 2–12 h created extremely high surface area spheres. These activated carbon spheres (ACS) possessed large fraction of fine pores (<1 nm), which makes them potential candidates for CO_2 capture.

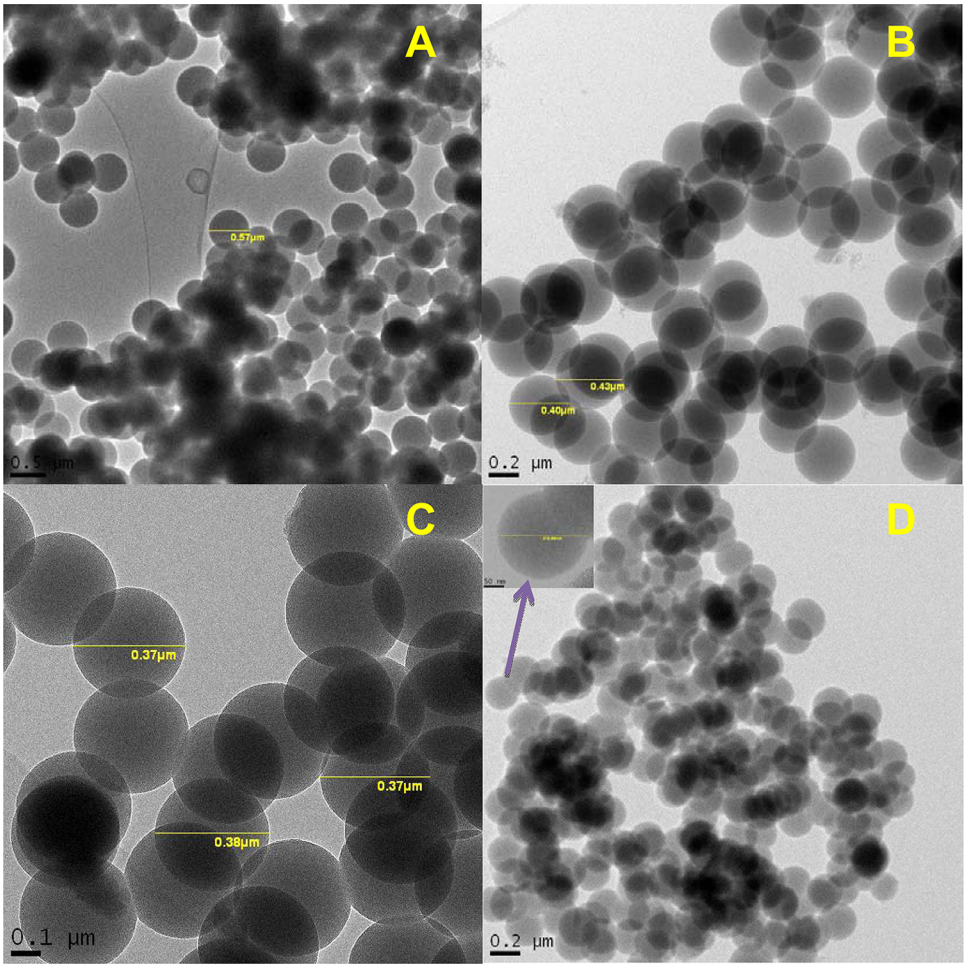

Figure 3. TEM images of CS-6 (A), CS-6-CD-4 (B), CS-6-CD-8 (C), and CS-6-CD-12 (D).

Nitrogen adsorption isotherms measured on these materials at −196 °C are presented in Figure 1; panels A, B, and C show isotherms for the CS samples obtained at three different carbonization temperatures (CS-T series), activated CS with CO_2 for 4 h (CS-T-CD-4 series), and CS-6 samples obtained by varying activation time (CS-6-CD-t series), respectively. The specific surface area and pore structure parameters are listed in Table 1. As can be seen from Figure 1 and Table 1, the ACS studied possessed very high surface area and total pore volume up to 2930 m^2/g and 1.1 cm^3/g, respectively. Importantly, the fraction of fine micropores (>1 nm) was significantly enhanced by CO_2 activation giving the micropore volumes of 0.33, 0.22, 0.22, and 0.19 cm^3/g for CS-4-CD-4, CS-6-CD-4, CS-8-CD-4, and CS-6-CD-8, respectively. However, nonactivated spheres showed relatively low N_2 adsorption and, thus, smaller surface area and micropore volume. Figure 1C and Table 1 show the effect of activation time of carbon spheres on the surface properties of the CS-6 series. As can be seen the surface area, total micropore volume and volume of fine micropores ($PV_{1\ nm}$) increase with increasing activation time. Pore size distribution (PSD) and cumulative pore volume curves obtained from N_2 adsorption by density functional theory (DFT) method for slit-like pore geometry are presented in Figures 2 and S1, Supporting Information, which show that all samples exhibit PSD curves, mainly located below 1.3 nm, indicating a great potential of these materials for CO_2 adsorption. As can be seen from Figure 2, the pore size and pore volume for the CS-T-CD-t series are increasing with increasing activation time. Both CS-6-CD-4 and CS-6-CD-8 show almost equal pore volumes in the range below 1 nm (~0.43 cm^3/g), which is reflected by similar values of the CO_2 uptake; however, CS-6-CD-8 exhibits the highest total pore volume (1.12 cm^3/g), mainly due to the presence of large micropores (above 1 nm). The CO_2 capture capability of these materials will be thoroughly discussed in the section devoted to CO_2 adsorption.

Morphology and Phase Structure. Transmission electron microcopy (TEM), thermogravimetric analysis (TGA), and X-ray diffraction (XRD) measurements were used to study the particle morphology and phase structure. As can be seen from Figure S2, Supporting Information, all samples showed spherical morphology with the average diameter of 610, 570, and 420 nm for as-synthesized polymer, CS-6 and CS-6-CD-4 carbon spheres, respectively. The smaller diameter of CS-6 is mainly due to the material shrinkage during carbonization. However, activation of CS-6 with CO_2 for 4 h at 850 °C resulted in carbon spheres with diameter of ~420 nm, indicating that a different chemical or physical phenomenon is taking place apart from material shrinkage. To better understand this observation, a series of activated samples was synthesized using CS-6 as carbon source and simply changing the activation time, while keeping the activation temperature constant at 850 °C. As shown on TEM images (Figure 3), the particle size is decreasing with increasing activation time, indicating deterioration of the outer surface of CS

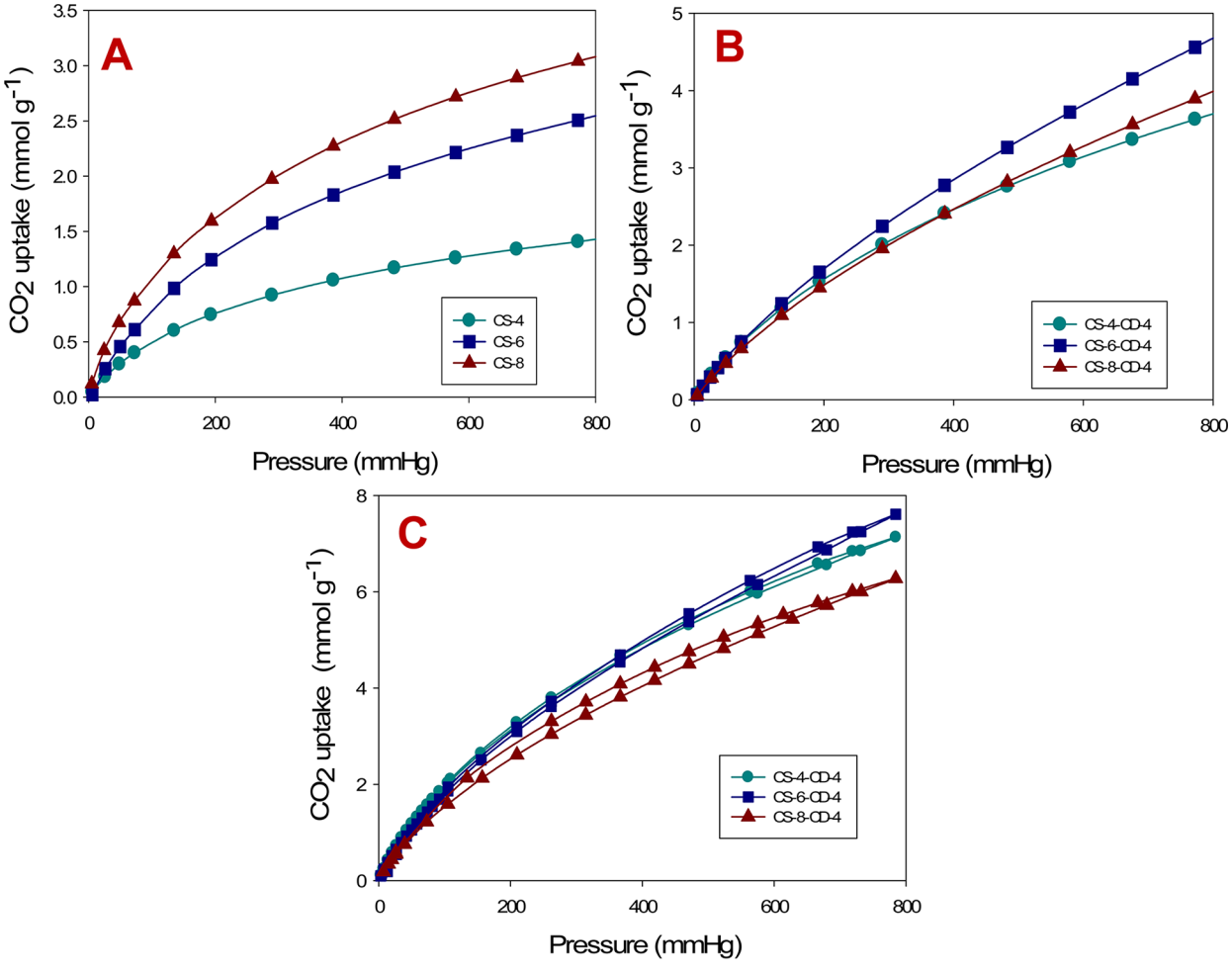

Figure 4. CO_2 adsorption isotherms for CS-T (nonactivated) (A) measured at 25 °C, for CS-T-CD-4 (B) measured at 25 °C, and for CS-T-CD-4 (C) measured at 0 °C.

with activation time. This deterioration is mainly due to reaction between CO_2 gas and the outer carbon surface of CS to form carbon monoxide. Interestingly, activation of these carbon spheres with CO_2 for about 12 h produced highly porous carbon spheres with the diameter around 200 nm. Therefore, the controlled activation of these carbon spheres can be employed to obtain ultraporous carbon spheres with the diameter even smaller than 200 nm. These carbon spheres can be introduced to the cell due to their smaller size and thus are potential materials for in vivo studies for drug delivery and cell imaging.

TGA analysis was employed to find the mass loss of carbons during the activation with respect to activation time. This analysis was carried out under similar conditions as activation in the furnace; a sample of CS was placed in the TGA pan under flowing CO_2 (50 cm^3/min) with a heating rate of 10 °C/min up to 850 °C and dwell for 12 h. As can be seen from Figure S3, Supporting Information, there is a considerable mass loss observed with increasing activation time. According to the TGA profiles, the mass losses for the CS-6-CD-2, CS-6-CD-4, CS-6-CD-8, and CS-6-CD-12 samples are 25, 40, 61, and 71, respectively.

The wide-angle X-ray diffraction (XRD) patterns for the CS studied are shown in Figure S4, Supporting Information. Two broad peaks at 2θ of around 25 and 44 degrees suggest that no pronounced graphitization occurred during carbonization and activation processes.[32]

CO_2 Adsorption and Isosteric Heat of Adsorption (Q_{st}). CO_2 adsorption on microporous carbon spheres was investigated at 25 and 0 °C under atmospheric pressure (1 bar). The CO_2 adsorption isotherms measured at ambient conditions for both nonactivated and activated samples are presented in Figure 4; panels A, B, and C show isotherms for CS-T (nonactivated), CS-T-CD-4 measured at 25 °C, and CS-T-CD-4 measured at 0 °C, respectively. As can be clearly seen from this figure, the CO_2 adsorption capacities are increasing with increasing carbonization temperature (Figure 4A). This observation is mainly due to the enlargement of the volume of fine micropores with increasing carbonization temperature (see Table 1). It is also noteworthy that the CS-8 sample exhibits a very high CO_2 uptake (1.42 mmol/g) at 0.2 bar and 25 °C (corresponding to flue gas conditions). This is mainly due to the presence of high fraction of ultrafine pores (<0.5 nm), which are responsible for low pressure adsorption at ambient temperature.[31] Activation of CS (CS-T series) produced highly microporous carbon spheres with fine pores (<1 nm). These ACS exhibited very high CO_2 adsorption capacities at ambient conditions; namely, CS-6-CD-4 showed the unprecedented CO_2 adsorption capacities of 4.55 and 7.48 mmol/g at 25 and 0 °C, respectively. To show the regeneration capability of the carbon sorbents studied, we have performed three runs of CO_2 adsorption/desorption measurements (see Figure S5, Supporting Information) and obtained almost identical isotherm curvess, indicating that these materials can be regenerated.

To find out the activation time effect on the CO_2 adsorption capacity, CO_2 adsorption measurements were performed for the CS-6-CD-t series of samples (Figure 5). As can be seen from Figure 5, the CO_2 capacity is increasing with increasing activation time for adsorption at 0 °C. However, at 25 °C, the CO_2 capacity initially increases with activation time to achieve a maximum, and after that, it decreases. The CS-6-CD-8 sample exhibited very high CO_2 adsorption capacities of 4.40 and 8.05 mmol/g at 25 and 0 °C, respectively. Although, CS-6-CD-8 possessed comparatively higher surface area than that of CS-6-CD-4 (see Table 1), these two samples showed similar CO_2 adsorption capacities because of almost equal volumes of fine micropores.

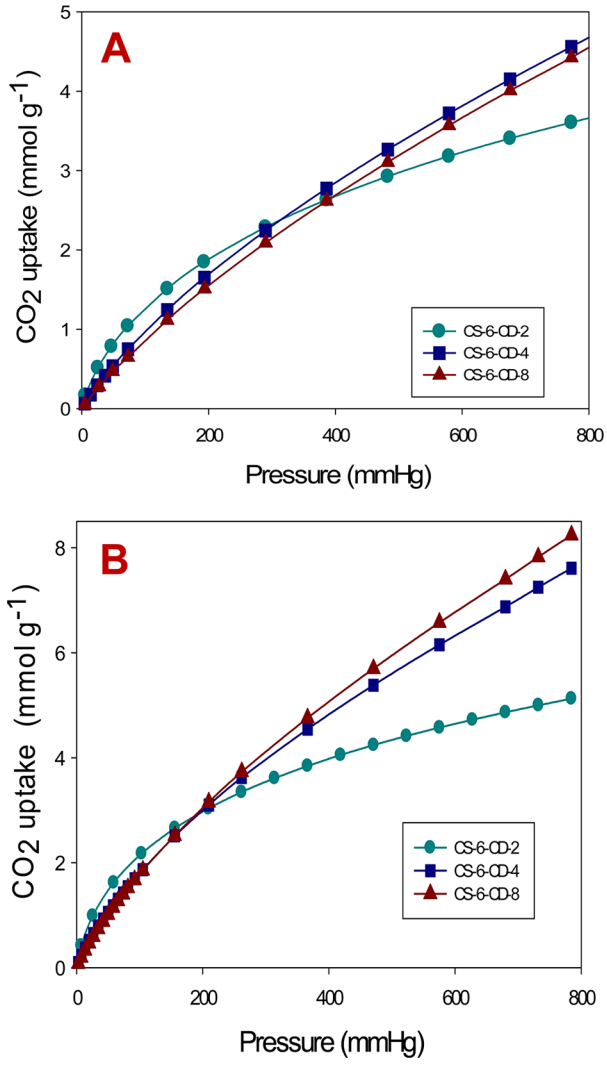

Figure 5. CO_2 adsorption isotherms for CS-6-CD-t measured at 25 °C (A) and 0 °C (B).

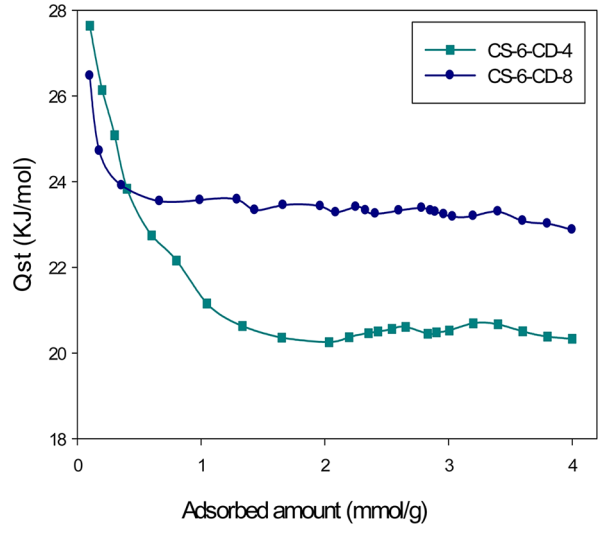

Figure 6. Isosteric heat of CO_2 adsorption on CS-6-CD-4 and CS-6-CD-8 calculated from the experimental adsorption isotherms at 0 and 25 °C.

dx.doi.org/10.1021/am400112m | ACS Appl. Mater. Interfaces 2013, 5, 1849−1855

The CO_2 isosteric heats of adsorption (Q_{st}) for CS-6-CD-4 and CS-6-CD-8 were calculated using adsorption isotherms obtained at 0 and 25 °C. The calculated Q_{st} for CS-6-CD-4 and CS-6-CD-8 are in the range of 27.7−20.3 and 26.5−22.9 kJ/mol, respectively, with the CO_2 amount adsorbed varying from 0.1 to 4.0 mmol/g (Figure 6). These ranges of values are relatively higher than those previously reported for various porous carbons[34−37] and higher or comparable to other adsorbents (MOF, zeolites, and silica materials),[38−40] which is due to the presence of fine micropores in the materials studied (see Table S1, Supporting Information).

CONCLUSIONS

A series of highly microporous carbon spheres has been prepared using a slightly modified Stöber method followed by controlled CO_2 activation. These activated carbon spheres possessed a large fraction of fine micropores (<1 nm) and high surface area, which resulted in an excellent CO_2 adsorption capacity at both ambient and low pressures. Notably, these carbon spheres exhibited very high CO_2 uptake of 8.05 and 4.55 mmol/g at 0 and 25 °C under 1 bar, respectively. Moreover, these carbons showed the relatively high CO_2 adsorption capacities at low CO_2 pressures, 1.42 mmol/g at 0.2 bar and 25 °C. Interestingly, activation of CS with CO_2 produced extremely microporous carbon spheres (BET surface area up to 2930 m^2/g) with the diameter around 200 nm, making them potentially attractive materials for biomedical applications such as adsorption, imaging, and drug release.[41]

ASSOCIATED CONTENT

Supporting Information

Table with CO_2 adsorption capacities and isosteric heats of adsorption for various sorbents and figures showing pore size distributions, thermogravimetric analysis data, SEM images, wide angle XRD data, and CO_2 adsorption isotherms for regenerated carbons. This material is available free of charge via the Internet at http://pubs.acs.org/.

AUTHOR INFORMATION

Corresponding Author

*Phone: 330-672-3790. Fax: 330-672-3816. E-mail: jaroniec@kent.edu.

Notes

The authors declare no competing financial interest.

ACKNOWLEDGMENTS

The TEM data were obtained at the (cryo) TEM facility at the Liquid Crystal Institute, Kent State University, supported by the Ohio Research Scholars Program *Research Cluster on Surfaces in Advanced Materials*. The authors thank Dr. Min Gao for technical support with the TEM experiments.

REFERENCES

(1) Samanta, A.; Zhao, A.; Shimizu, G. K. H.; Sarkar, P.; Gupta, R. *Ind. Eng. Chem. Res.* **2012**, *51*, 1438−1463.
(2) D'Alessandro, D.; Smit, B.; Long, J. *Angew. Chem., Int. Ed.* **2010**, *49*, 6058−6082.
(3) Haszeldine, R. S. *Science* **2009**, *325*, 1647−1652.
(4) Jee, S. E.; Sholl, D. S. *J. Am. Chem. Soc.* **2009**, *131*, 7896−7904.
(5) Su, F.; Lu, C.; Kuo, S.; Zeng, W. *Energy Fuels* **2010**, *24*, 1441−1448.
(6) Zukal, A.; Zones, S. I.; Kubu, M.; Davis, T. M.; Cejka, J. *ChemPlusChem* **2012**, *77*, 675−681.
(7) Millward, A. R.; Yaghi, O. M. *J. Am. Chem. Soc.* **2005**, *127*, 17998−17999.
(8) Walton, K. S.; Millward, A. R.; Dubbeldam, D.; Frost, H.; Low, J. J.; Yaghi, O. M.; Snurr, R. Q. *J. Am. Chem. Soc.* **2008**, *130*, 406−407.
(9) Sumida, K.; Rogow, D. L.; Mason, J. A.; McDonald, T. M.; Bloch, E. D.; Herm, Z. R.; Bae, T.; Long, J. R. *Chem. Rev.* **2012**, *112*, 724−781.
(10) Liu, J.; Thallapally, P. K.; McGrail, B. P.; Brown, D. R.; Liu, J. *Chem. Soc. Rev.* **2012**, *41*, 2308−2322.
(11) Ren, J.; Wu, L.; Li, B. *Ind. Eng. Chem. Res.* **2012**, *51*, 7901−7909.
(12) Zukal, A.; Jagiello, J.; Mayerova, J.; Cejka, J. *Phys. Chem. Chem. Phys.* **2011**, *13*, 15468−15475.
(13) Yu, J.; Le, Y.; Cheng, B. *RSC Adv.* **2012**, *2*, 6784−6791.
(14) Rabbani, M. G.; El-Kaderi, H. *Chem. Mater.* **2012**, *24*, 1511−1517.
(15) Ben, T.; Ren, H.; Ma, S.; Cao, D.; Lan, J.; Jing, X.; Wang, W.; Xu, J.; Deng, F.; Simmons, J.; Qiu, S.; Zhu, G. *Angew. Chem., Int. Ed.* **2009**, *48*, 9457−9460.
(16) Koirala, R.; Gunugunuri, K. R.; Pratsinis, S. E.; Smirniotis, P. G. *J. Phys. Chem. C* **2011**, *115*, 24804−24812.
(17) Wang, Q.; Tay, H. H.; Zhong, Z.; Luo, J.; Borgna, A. *Energy Environ. Sci.* **2012**, *5*, 7526−7530.
(18) Broda, M.; Müller, C. R. *Adv. Mater.* **2012**, *24*, 3059−3064.
(19) Silvestre-Albero, J.; Wahby, A.; Sepulveda-Escribano, A.; Martinez-Escandell, M.; Kaneko, K.; Rodriguez-Reinoso, F. *Chem. Commun* **2011**, *47*, 6840−6842.
(20) Zhou, J.; Li, W.; Zhang, Z.; Xing, W.; Zhuo, S. *RSC Adv.* **2012**, *2*, 161−167.
(21) Yazaydin, A. O.; Snurr, R. Q.; Park, T.; Koh, K.; Liu, J.; LeVan, M. D.; Benin, A. I.; Jakubczak, P.; Lanuza, M.; Galloway, D. B.; Low, J. J.; Willis, R. R. *J. Am. Chem. Soc.* **2009**, *131*, 18198−18199.
(22) Furukawa, H.; Ko, N.; Go, Y. B.; Aratani, N.; Choi, S. B.; Choi, E.; Yazaydin, A. Ö.; Snurr, R. Q.; O'Keeffe, M.; Kim, J.; Yaghi, O. M. *Science* **2010**, *329*, 424−428.
(23) Küsgens, P.; Rose, M.; Senkovska, I.; Fröde, H.; Henschel, A.; Siegle, S.; Kaskel, S. *Microporous Mesoporous Mater.* **2009**, *120*, 325−330.
(24) Hao, G.; Li, W.; Qian, D.; Lu, A. *Adv. Mater.* **2010**, *22*, 853−857.
(25) Plaza, M. G.; Gonzalez, A. S.; Pevida, C.; Pis, J. J.; Rubiera, F. *Appl. Energy* **2012**, *99*, 272−279.
(26) Wang, J.; Heerwig, A.; Lohe, M. R.; Oschatz, M.; Borchardt, L.; Kaskel, S. *J. Mater. Chem.* **2012**, *22*, 13911−13913.
(27) Yang, H.; Yuan, Y.; Tsang, S. C. E. *Chem. Eng. J.* **2012**, *185−186*, 374−379.
(28) Xing, W.; Liu, C.; Zhou, Z.; Zhang, L.; Zhou, J.; Zhuo, S.; Yan, Z.; Gao, H.; Wang, G.; Qiao, S. Z. *Energy Environ. Sci.* **2012**, *5*, 7323−7327.
(29) Hu, X.; Radosz, M.; Cychosz, K. A.; Thommes, M. *Environ. Sci. Technol.* **2011**, *45*, 7068−7074.
(30) Yang, Q.; Zhong, C. *Can. J. Chem. Eng.* **2004**, *82*, 580−589.
(31) Presser, V.; McDonough, J.; Yeon, S.; Gogotsi, Y. *Energy Environ. Sci.* **2011**, *4*, 3059−3066.
(32) Wickramaratne, N. P.; Jaroniec, M. *J. Mater. Chem. A* **2013**, *1*, 112−116.
(33) Liu, J.; Qiao, S. Z.; Liu, H.; Chen, J.; Orpe, A.; Zhao, D.; Lu, G. Q. *Angew. Chem., Int. Ed.* **2011**, *50*, 5947−5951.
(34) Guo, B.; Chang, L.; Xie, K. *J. Nat. Gas Chem.* **2006**, *15*, 223−229.
(35) Jin, Y.; Lee, D.; Lee, S.; Moon, W.; Jeon, S. *Anal. Chem.* **2011**, *83*, 7194−7197.
(36) Ben, T.; Li, Y.; Zhu, L.; Zhang, D.; Cao, D.; Xiang, Z.; Yao, X.; Qiu, S. *Energy Environ. Sci.* **2012**, *5*, 8370−8376.
(37) Nandi, M.; Okada, K.; Dutta, A.; Bhaumik, A.; Maruyama, J.; Derks, D.; Uyama, H. *Chem. Commun.* **2012**, *48*, 10283−10285.
(38) Zukal, A.; Dominguez, I.; Mayerova, J.; Cejka, J. *Langmuir* **2009**, *25*, 10314−10321.
(39) An, J.; Geib, S. J.; Rosi, N. L. *J. Am. Chem. Soc.* **2010**, *132*, 38−39.

(40) Grajciar, L.; Cejka, J.; Zukal, A.; Areán, C. O.; Palomino, G. T.; Nachtigall, P. *ChemSusChem* **2012**, *5*, 2011−2022.
(41) Tanaka, C.; Ohtani, H.; Tsujimoto, M.; Ohdo, S.; Taniguchi, M.; Mizooku, Y.; Saitoh, Y.; Kimura, M.; Uchimaru, H.; Irie, S.; Sawada, Y. *J. Clin. Pharmacol.* **2007**, *47*, 904−908.